Mathematical Morphology in the L*a*b* Colour Space

Allan Hanbury* and Jean Serra

30 August 2001

Technical report N-36/01/MM
Centre de Morphologie Mathématique
Ecole des Mines de Paris
35, rue Saint-Honoré
77305 Fontainebleau cedex
France

*Hanbury@cmm.ensmp.fr

Abstract

The use of mathematical morphology in the L*a*b* colour space is discussed. Initially, a description of the characteristics of the L*a*b* space and a comparison to the HLS space are given. This is followed by a theoretical demonstration of the use of weighting functions to impose a complete order on a vector space. Various colour weighting functions are considered, and one based on a model of an electrostatic potential is chosen for further development. A lexicographical order using this weighting function allows one to simulate a complete order by colour saturation, a notion absent from the definition of the L*a*b* space. Demonstrations of the basic morphological operators and of the top-hat operator making use of the proposed colour order are shown.

Keywords: L*a*b* colour space, mathematical morphology, lexicographical order, vector order, vector weighting function, electrostatic potential.

Mots clés: Espace couleur L*a*b*, morphologie mathématique, ordre lexicographique, ordre vectoriel, fonction de ponderation de vecteurs, potentiel électrostatique.

Contents

1. Introduction

Much research has been carried out on the application of mathematical morphology [12, 14] to colour images, a subset of the research on its application to multivariate data [13, 15]. While the definition of orders for vectors in the RGB colour space [5, 6] has been discussed, these formulations usually present the disadvantage of having to arbitrarily choose one of the red, green or blue channels to play a dominant role in the ordering. Attempts have been made to overcome this limitation through the use of, for example, bit-interlacing [4]. The application of mathematical morphology in a colour space which has an angular hue component [9] can overcome this disadvantage, allowing a non-constrained choice of the dominant hue, or permitting the implementation of rotationally invariant operators independent of the hue [8]. The use of lexicographical orders in the HLS colour space [7] allow the pixels to be ordered by physically intuitive characteristics such as luminance, saturation or hue difference.

However, the HLS space suffers from a number of disadvantages such as an uneven distribution of the hue values when converting from a rectangular coordinate system such as RGB [7, chapter 2]. As this space is closely linked to the RGB representation, it is also device-dependent, that is, the colour coordinates depend on the characteristics of the devices used to capture and display the images.

The CIE (Commission Internationale de l'Eclairage), in 1976, introduced two device-independent spaces, the L*a*b* and L*u*v* spaces. They were designed to be perceptually uniform, meaning that colours which are visually similar are close to each other in the colour space (if the proper distance metric is used). These spaces are based on the CIE-XYZ space, which allows one to take into account the illumination characteristics of an image. The L*a*b* space is often used in scientific imaging and colourimetry, as the use of properly calibrated instruments allows the exchange of objectively measured colour information between different observers. Nevertheless, a transformation from the RGB space to the L*a*b* space results in an irregularly shaped gamut of colours, its shape being dependent on the illumination conditions, and which lacks the notion of colour saturation. It is thus difficult to apply standard morphological operators to assist in making measurements. In addition, a transformation back to a rectangular coordinate system often results in the loss of some colour information.

In this report, we begin with a discussion of the L*a*b* space and its characteristics (chapter 2). Due to the irregular shape of the L*a*b* space colour gamut, we consider the use of a weighting function in the space which imposes a colour vector order analogous to an order by saturation in the HLS space (chapter 3). Examples of the use of the basic morphological operators as well a top-hat operator are shown. Chapter 4 concludes.

2. The L*a*b* space

Before applying image analysis operators to an image represented in a certain colour space, it is useful to know the characteristics of the colour space. This helps avoid unexpected behaviour of the operators due to colour space particularities. The characteristics of the L*a*b* space are examined in detail in this chapter. Sections 2.1 to 2.3 provide basic information on the colour space, and sections 2.4 and 2.5 examine the component distributions and the relation of the L*a*b* space to the HLS space.

2.1. Description

The L*a*b* space is one of two device-independent colour spaces developed by the CIE to be approximately perceptually uniform. This means that colours which appear similar to an observer are located close to each other in the L*a*b* coordinate system.

In the L*a*b* colour space:

- L^* represents the lightness (luminance).
- a^* encodes the red-green sensation, with positive a^* indicating a red colour, and negative a^* a green colour.
- b^* encodes the yellow-blue sensation, with positive b^* indicating yellow and negative b^* indicating blue.

The grey-levels or colourless points are located on the luminance axis $(a^* = 0, b^* = 0)$, with black at $L^* = 0$, and white at $L^* = 100$. The colour characteristics are summarised schematically in figure 2.1. As is clear, it is possible to define a polar representation of the chrominance coordinates. The chroma C^* and hue h^* are defined as

$$C^* = \left[(a^*)^2 + (b^*)^2\right]^{\frac{1}{2}}$$

and

$$h^* = \arctan\left(\frac{b^*}{a^*}\right)$$

The hue h^* is obviously an angular value, and has the property that $h^* = h^* + 2\pi n,\ n \in \mathbb{Z}$. Combining the C^* and h^* coordinates with L^* leads to a cylindrical representation of the L*a*b* space.

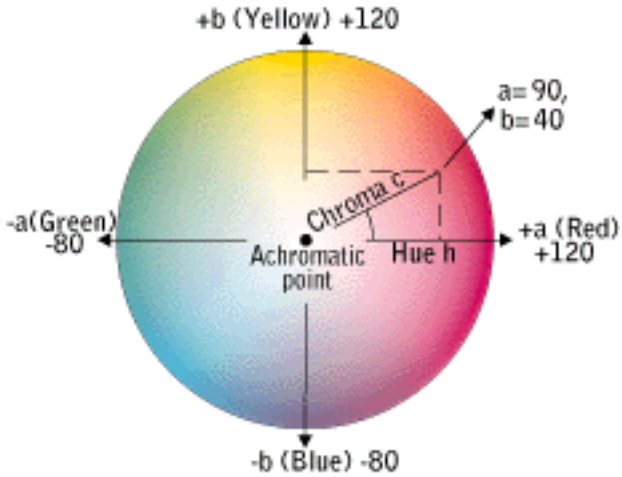

Figure 2.1.: A schematic representation of the chrominance information in the L*a*b* colour space (from [1]).

2.2. Colour difference

The total colour difference ΔE^*_{ab} between two colours, each expressed in terms of L^*, a^* and b^* is given by the Euclidean metric

$$\Delta E^*_{ab} = \left[(\Delta L^*)^2 + (\Delta a^*)^2 + (\Delta b^*)^2\right]^{\frac{1}{2}} \tag{2.1}$$

In the cylindrical representation, the Euclidean distance between two colours (L^*_1, h^*_1, C^*_1) and (L^*_2, h^*_2, C^*_2), is

$$\Delta E^*_{ab} = \left[(\Delta L^*)^2 + C^*_1 + C^*_2 - 2C^*_1 C^*_2 \cos(\Delta h^*)\right]^{\frac{1}{2}} \tag{2.2}$$

where $\Delta h^* = (h^*_1 - h^*_2)$.

The perceptual uniformity of the L*a*b* space implies that if, for two colours, ΔE^*_{ab} is small, then the colours are visually similar.

2.3. Transformation from RGB to L*a*b*

The transformation from the RGB to the L*a*b* colour space is done by first transforming to the CIE XYZ space, and then to the L*a*b* space. The details of this transformation are given, for both directions, in appendix A.

Before doing the transformation from RGB to XYZ, one needs to specify the coordinates of the three primary colour stimuli and of the white point (the nominally white object-colour stimulus) in the XYZ space. The primary colour stimuli depend on the hardware characteristics of the image capture device (i.e. the camera). The white point is usually specified by the spectral radiant power of one of the CIE standard illuminants, such as D_{65} (daylight) or A (tungsten filament lamp), reflected into the observer's eye by the perfect reflecting diffuser [16]. If one knows the

illumination conditions used when acquiring the image, then the specification of the white point is simple. If the illumination conditions are unknown, a hypothesis can be made, or a technique for estimating the white point from the image [3] can be used. For all the transformations in this report, the primary colour stimuli and D_{65} white point specified in the Rec. 709 HDTV standard [11] have been used. These correspond closely to the display characteristics of computer monitors. The coordinates of the Rec. 709 primaries and white point are given in appendix A.

2.4. Characteristics of the L*a*b* space

The transformation from an RGB cube completely filled with points does not fill the L*a*b* space, but produces a gamut of colours whose shape depends on the primaries and white point. In this section, we investigate the shape of the resultant colour gamut. This analysis is performed for the specific case of an RGB space transformed to the L*a*b* space using the Rec. 709 standard primaries and white point, but can easily be adapted to other situations.

2.4.1. Component distributions

An analysis of the component distributions in the L*a*b* space can give an idea of the shape of the colour gamut. This is similar to the analysis of the HLS space in [7]. To allow the distributions of the L*a*b* components to be visualised, a transformation from an RGB colour cube containing points equally spaced by $\frac{1}{100}$ throughout the region $[0,1] \times [0,1] \times [0,1]$ to the L*a*b* space is done. For each point $[R, G, B]$, the corresponding values of L^*, a^*, and b^*, C^* and h^* are rounded to the nearest integer and the corresponding bins in the histograms are incremented. The L^*, C^*, h^*, a^* and b^* histograms are shown in figure 2.2.

The C^*, L^*, a^* and b^* distributions are all smooth, with the peaks of the a^* and b^* distributions close to zero. The chrominance distribution shows that there are very few pixels which are on the luminance axis (i.e. at $C^* = 0$). A comparison of the hue distribution with the corresponding distribution for the HLS space [7] shows that the L*a*b* hue component h^* does not suffer from regularly spaced spikes in the histogram like the HLS hue component H. However, the h^* component does not have a flat distribution, and there are some values of h^* which appear to have an excess of pixels assigned to them. This is examined further by calculating a two-dimensional chrominance histogram.

For the calculation of the two-dimensional chrominance histogram, the transformation from an RGB colour cube containing points equally spaced by $\frac{1}{256}$ throughout the region $[0,1] \times [0,1] \times [0,1]$ to the L*a*b* space is done. For each point $[R, G, B]$, the resulting coordinates a^* and b^* are rounded to the nearest integer, and the bin $[a^*, b^*]$ of the histogram is incremented. A plot of the histogram is shown in figure 2.3. In this image, the grey-level at each point $[a^*, b^*]$ indicates the number of pixels in the RGB cube mapped to this point. In the full three-dimensional L*a*b* space, these pixels would be mapped to different luminance values. However, this two-dimensional histogram allows one to make some useful observations:

1. The largest number of points are concentrated near the origin, the position of the luminance axis

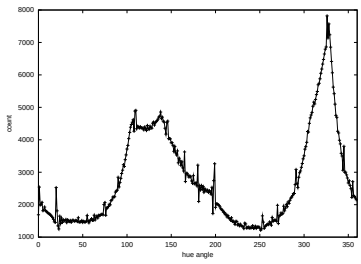

(a) Hue h^*

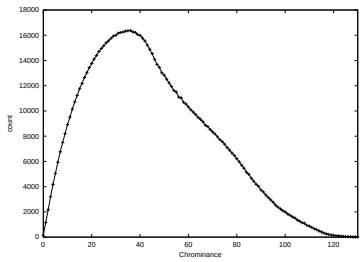

(b) Chrominance C^*

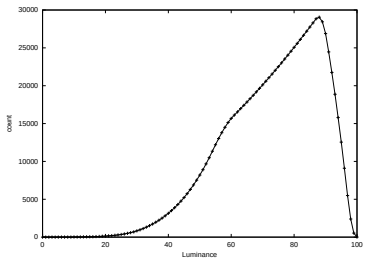

(c) Luminance L^*

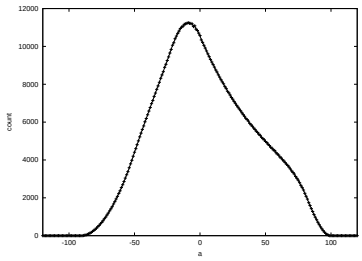

(d) a^*

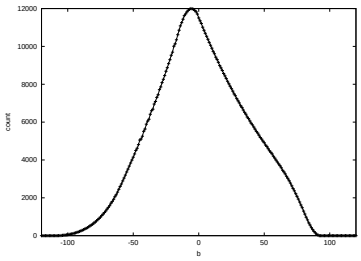

(e) b^*

Figure 2.2.: The histograms of the Hue h^*, Chrominance C^* and Luminance L^*, and the chrominance Cartesian coordinates a^* and b^* calculated from a set of equally-spaced points filling an RGB cube.

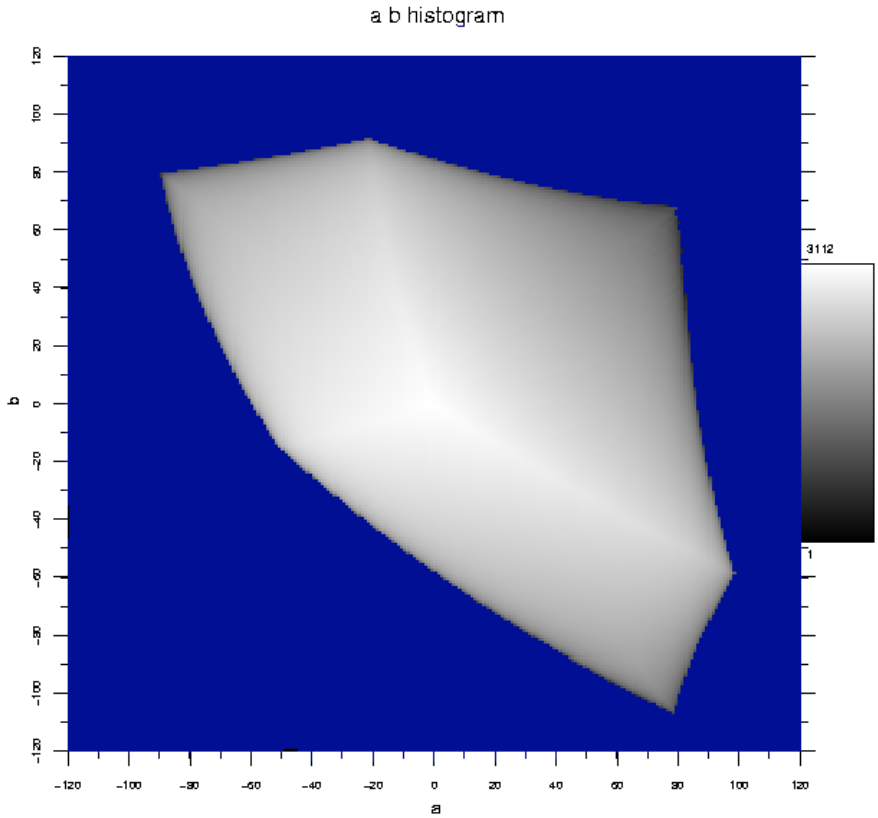

Figure 2.3.: The a^*b^* histogram which results from transforming an RGB cube to the L*a*b* space. The grey-level at each point $[a^*, b^*]$ indicates the number of pixels in the RGB cube mapped to this point. The zero-valued regions are indicated in blue.

2. The distribution of colours is not circular — the maximum value assumed by C^* depends on h^*.

2.4.2. Extrema

The extremal points of the L*a*b* colour gamut are those points which are furthest away from the luminance axis, that is, the points with the maximum values of C^*. These extrema can be seen on the histogram in figure 2.3. It is, however, interesting to find the luminance value corresponding to each of these extremal chroma points.

For the transformation from the RGB cube, for each integer value of h^*, the point with the largest chroma C^* is found. In figure 2.4, the value of C^* is plotted for the extremal points corresponding to each integer value of h^*, along with the luminance L^* of the extremal point. These functions are henceforth denoted as $C_{\text{ext}}(h)$ and $L_{\text{ext}}(h)$, where the values can be read off the graph for integer values of h^*, and interpolated for non-integer values.

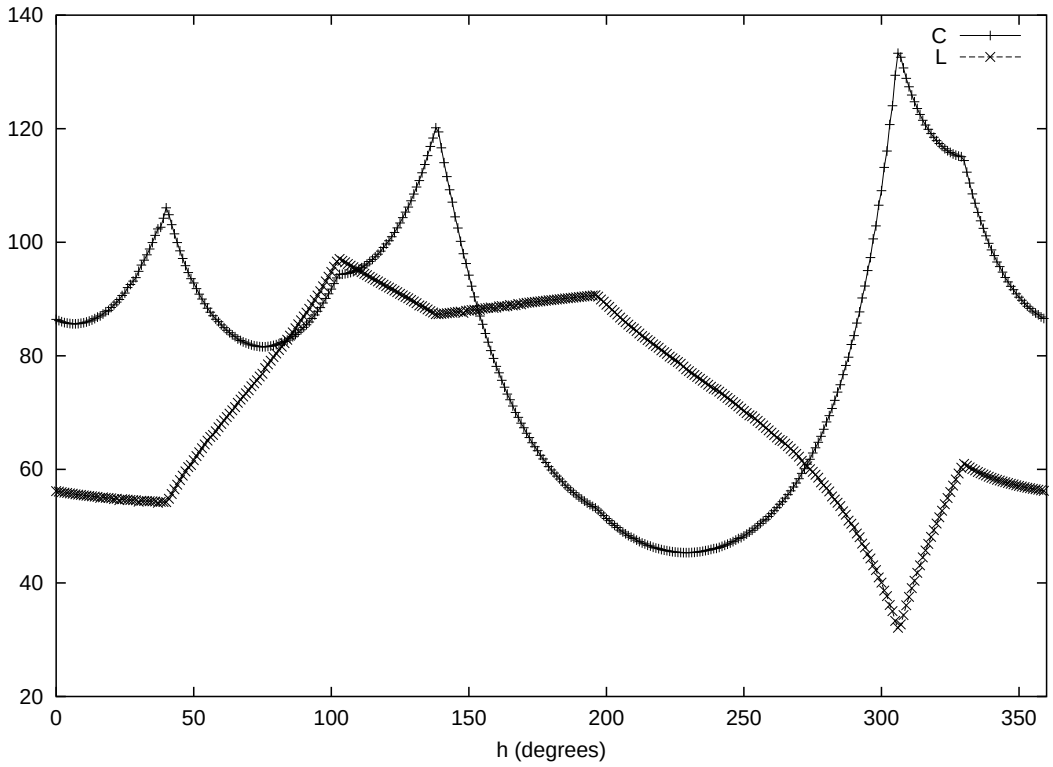

Figure 2.4.: The values of the extrema of the chroma C^* and their corresponding luminance L^* as a function of hue h^* in the L*a*b* space.

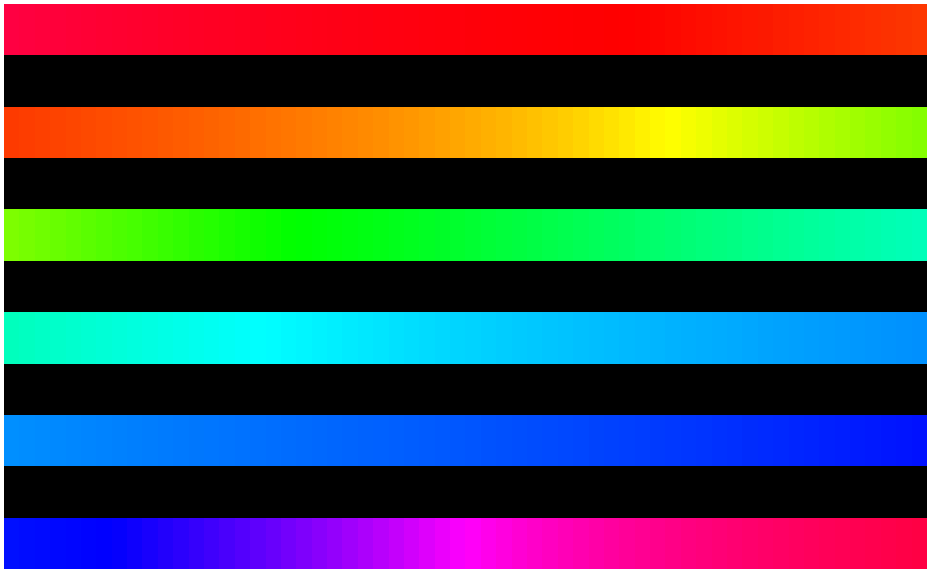

Figure 2.5.: The colours corresponding to the extremal C^* values. The first line has values of h^* from $0°$ to $59°$, the second from $60°$ to $119°$, etc.

2.5. Comparison between the HLS and L*a*b* spaces

In the HLS (double-cone) space, the points with highest saturation ($S = 1$) have luminance values of half the maximum ($L = \frac{1}{2}$). It is interesting to examine the relation between these points and the extremal chroma points in the L*a*b* colour gamut. For the case we are treating, where use is made of primaries and a white point well adapted to computer monitors, the extrema of the two spaces should coincide.

The extremal chroma points of the L*a*b* colour gamut are those plotted in figure 2.4, and the colours corresponding to these points for integer hues between $0°$ and $360°$ are shown in figure 2.5. The h^*, L^* and C^* values corresponding to these colours are shown in the grey-level images in figure 2.6.

To test that the extremal points of the L*a*b* colour gamut correspond to those of the HLS space, figure 2.5 was converted to the HLS space (via the RGB space). These H, L and S components are shown in figure 2.7. The values for all the pixels in the L band (figure 2.7b) are $\frac{1}{2}$, and for all the pixels in the S band (figure 2.7c) are 1. Apart from a small displacement of the hue origin between the two spaces, it is clear that the extremal points of the L*a*b* colour gamut correspond exactly to the points of highest saturation in the HLS space.

2.6. Notation

In this report, we deal with a colour image in the L*a*b* space

$$f : \mathbb{Z}^2 \to \mathbb{R}^3 : \mathbf{x} = (x, y) \to \mathbf{c} = (L^*, a^*, b^*)$$

(a) h^*

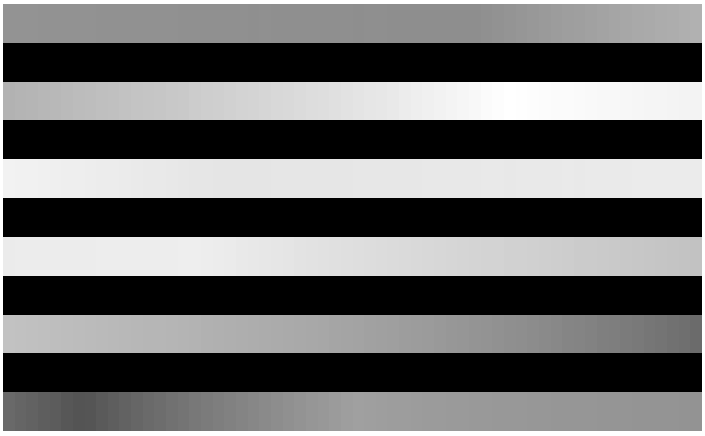

(b) L^*

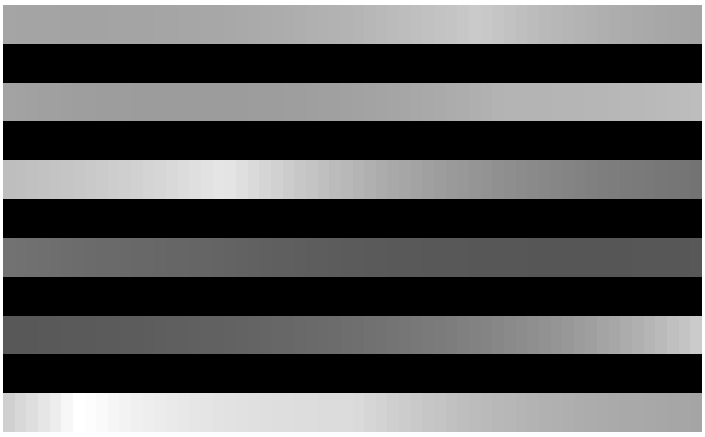

(c) C^*

Figure 2.6.: The h^*, L^* and C^* bands of the image in figure 2.5.

(a) H

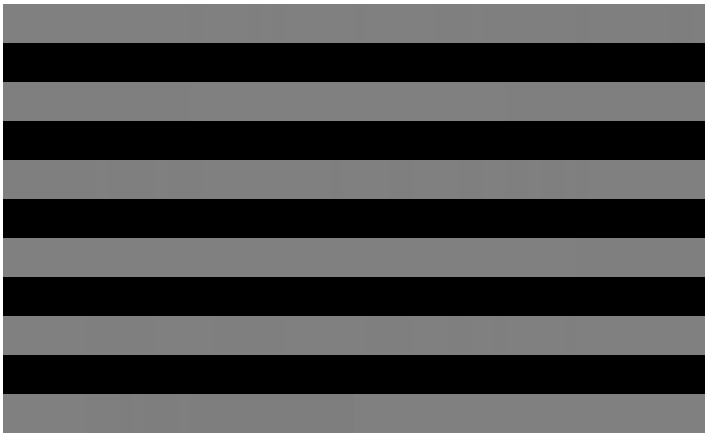

(b) L

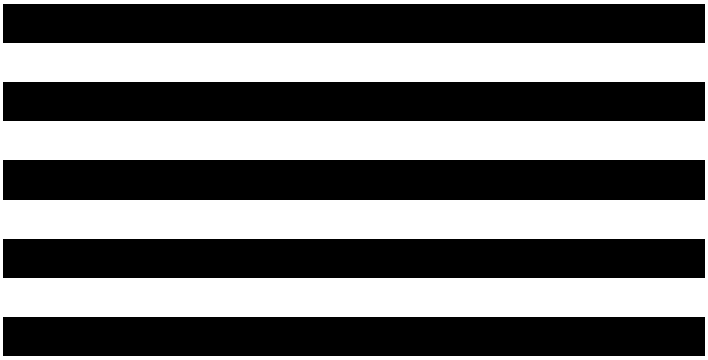

(c) S

Figure 2.7.: The H, L and S bands of the colour image in figure 2.5, obtained by transforming the image to the RGB space and then to the HLS space.

or its associated polar representation

$$f : \mathbb{Z}^2 \rightarrow \mathbb{R}^3 : \mathbf{x} = (x, y) \rightarrow \mathbf{c} = (L^*, h^*, C^*)$$

where $0° \leq h^* \leq 360°$. The components of the two possible representations are written $L^*(\mathbf{x})$, $a^*(\mathbf{x})$, $b^*(\mathbf{x})$, $h^*(\mathbf{x})$ and $C^*(\mathbf{x})$.

To simplify the notation in some sections, we assign an index i to each of the n vectors in the image, written as $\mathbf{c}_i = (L^*, a^*, b^*)_i$. The individual components of the vector with index i are written as L_i^*, a_i^*, b_i^*, h_i^* and C_i^*. B is a structuring element, and $B_{\mathbf{x}}$ indicates the structuring element at point $\mathbf{x}$ in the image.

3. Mathematical Morphology

The L*a*b* space does not have a notion of colour saturation. Nevertheless, we have shown in the previous chapter that for the chosen set of primaries and white point, the most highly saturated points in the HLS space correspond to the extremal points of the L*a*b* colour gamut. In this chapter, we make use of this and of the fact that the least saturated points are found on the luminance axis to develop an analogue to the lexicographical order by saturation described in [7].

Due to the irregular shape of the L*a*b* colour gamut, one cannot simply, in analogy with the HLS space, define the supremum to be the pixel with the largest value of C^*, as the maximum possible value of C^* varies with hue. We therefore proceed by defining a weighting function which assigns a weight to each colour based on its distance to an extremal colour. In Section 3.1, the theory relating to the use of weighting functions for colour morphology (or morphology on vector-valued images) is presented. The development leading to the choice of a good weighting function is given in section 3.2, and the use of this weighting function in morphological operators is demonstrated in section 3.3. Lastly, the top-hat (section 3.4), statistics on the lexicographical order (section 3.5) and rotational invariance (section 3.6) are discussed.

3.1. Colour morphology theory

We know that the morphological operators are expressed as products of the suprema and infima of the elements of the lattice under study. When we deal with numerical functions in $\mathbb{R}^n$ or $\mathbb{Z}^n$, which also form a vector space, we append additions and multiplication to the operators used. In practice, we are always led to take the biggest or smallest value of a family with a finite number of elements, a value which obviously belongs to the family.

However, once we define the lattice $\mathcal{L}$ as the product of two numerical lattices, lets say R and G for red and green, this property ceases to be true. The supremum of $(r_1 = 10, g_1 = 1)$ and $(r_2 = 1, g_2 = 10)$ is $(10, 10)$, different from the two operands. The proposition developed here indicates the conditions under which one has the desirable property of "remaining in the family". We formulate it in the general framework of a compact lattice with closed order, which has the advantage of modelling all the colour spaces, and also allows us to place ourselves in $\mathbb{R}^n$ or $\mathbb{Z}^n$. A lattice $\mathcal{L}$ is called topological if we assign it a topology, and its order is closed if two families $\{x_i, y_i, i \in I\}$ satisfy $x_i \leq y_i$, $x_i \to x$, $y_i \to y$ in $\mathcal{L}$, then $x \leq y$.

A family $\{x_i, i \in I\}$ in a lattice $\mathcal{L}$ is filtering increasing (resp. decreasing) if the set of indices I has an order relation verifying the following two properties:

1. $i > j \Rightarrow x_i > x_j$ (resp. $x_i < x_j$)

2. For every $i, j \in I$, there exists a $k \in I$ which is bigger the i and j.

We also note that in a complete lattice $\mathcal{L}$, the notion of a monotone limit of a filtering increasing (resp.decreasing) family $\{a_i, i \in I\}$, i.e.

$$m_1 = \vee a_i \qquad (\text{resp. } m_0 = \wedge a_i) \tag{3.1}$$

is purely algebraic, and does not use any topology ([10], pg. 16).

Finally, Matheron showed that if the complete lattice $\mathcal{L}$ is completely ordered, it permits a unique topology which renders it compact with closed order (CCO) ([10], criterion 6-1). This topology satisfies the following two equivalent properties ([10], theorem 5-2)

1. The monotone and topological limits coincide (i.e. equation 3.1 is equivalent to $a_i \to m$).

2. When the family $\{a_i\}$ is closed in $\mathcal{L}$, the operators $\{a_i\} \to \vee a_i$ and $\{a_i\} \to \wedge a_i$ are continuous.

These preliminaries lead to the property for which we are aiming, that is

Proposition *Let $\mathcal{L}$ be a complete lattice, and $\{a_i, i \in I\}$ an arbitrary family of elements of $\mathcal{L}$, with $m_0 = \wedge a_i$ and $m_1 = \vee a_i$. The elements m_0 and m_1 belong to the family $\{a_i\}$ (finite or not) if and only if the lattice $\mathcal{L}$ is completely ordered and $\{a_i\}$ is a closed subset of $\mathcal{L}$.*

Proof *Suppose that $\mathcal{L}$ is completely ordered. All filtering families $\{a_i, i \in I\}$ of elements are ordered in the lattice by decreasing values $\{a_i^0\}$, and by increasing values $\{a_i^1\}$. For the unique topology CCO induced on $\mathcal{L}$ by its complete order, we have, by theorem 5-2 of Matheron*

$$a_i^0 \to m_0 = \wedge a_i \quad \text{and} \quad a_i^1 \to m_1 = \vee a_i$$

If we assume that the family $\{a_i\}$ is closed, and hence that it contains its adherent points, we have $m_0 \in \{a_i\}$ and $m_1 \in \{a_i\}$.
Conversely, suppose that $\mathcal{L}$ contains a class of families $\mathcal{F}$ which contain their extremal elements. As this class contains the finite families, by hypothesis, it contains all the pairs of elements, which are therefore all comparable. It follows from this that the lattice $\mathcal{L}$ is completely ordered, and from the Matheron criterion that the class of families $\mathcal{F}$ is the class of closed sets of $\mathcal{L}$. ∎

The proposition says that we must use a completely ordered lattice, without imposing a particular one. Therefore any lattice derived from a convenient one by an order-preserving bijection is also usable. This allows a large number of solutions.

When we apply this proposition to a colour space, L*h*C* for example, it shows that if we do not want to generate new colours, it is essential to construct a scalar function $w : (L^*, h^*, C^*) \to \overline{\mathbb{R}}$ for which we can construct the suprema and infima. The proposition does not give any indication on the physical pertinence of a function w, but guarantees that the procedure is sufficient if w is injective. As this is not generally the case, it is necessary to complete the

numerical order of w, so that one can order the points (L_i^*, h_i^*, C_i^*) and $\left(L_j^*, h_j^*, C_j^*\right)$ where $w\left(L_i^*, h_i^*, C_i^*\right) = w\left(L_j^*, h_j^*, C_j^*\right)$. One can, for example, use cascades of lexicographical orders, possibly dependent on the values of w. In this new completely ordered lattice, the function w is replaced by a composite function u, bi-unique, which permits one to assign a triplet (L^*, h^*, C^*) to a supremum or infimum of $\{u_i\}$.

3.2. The weighting function

In this section, we develop a weighting function allowing the colour vectors to be ordered, as discussed in section 3.1. The weighting function w associates a weight w_i with each colour $\mathbf{c}_i$

$$w : \mathbb{R}^3 \to \mathbb{R} : \mathbf{c}_i = (L^*, h^*, C^*)_i \to w_i$$

It is defined so that a lower weight implies a colour closer to the extremal points (more highly saturated), and a higher weight indicates a colour close to the luminance axis (less saturated).

Four possible methods of defining weighting functions are discussed. The three methods based on distance functions are rejected for reasons discussed in section 3.2.1, whereas the best weighting function was found to be one modelled on an electrostatic potential, the details of which are given in section 3.2.2.

3.2.1. Distance methods

Two possible methods were considered and rejected. The first is to measure the distance from a colour in the L*a*b* space to the extremal point with the same hue. In symbolic form, the weighting w_i of each colour point $(L^*, h^*, C^*)_i$ is calculated as

$$w_i = \left\{[L_i^* - L_{\text{ext}}\left(h_i^*\right)]^2 + [C_i^* - C_{\text{ext}}\left(h_i^*\right)]^2\right\}^{\frac{1}{2}} \tag{3.2}$$

where $C_{\text{ext}}\left(h\right)$ and $L_{\text{ext}}\left(h\right)$ are the extremal points (section 2.4.2). However, this approach does not work as the L*a*b* colour gamut is not spherical. A two-dimensional illustration of this problem is shown in figure 3.1. The extremal points of a simple two-dimensional non-circular space with centre o are shown. Using a two-dimensional version of equation 3.2, point a would be assigned a weight w_a equal to the distance d, the distance to the extremal point with the same hue. However, the distance to the closest extremal point is actually e. This form of weighting function therefore assigns too high a weight to some colours.

The second distance-based approach attempts to overcome the previous limitation by setting the weight as the distance to the closest extremal point, or

$$w_i = \inf_{0^\circ \leq h \leq 360^\circ} \left\{[L_i^* - L_{\text{ext}}\left(h\right)]^2 + [C_i^* - C_{\text{ext}}\left(h\right)]^2\right\}^{\frac{1}{2}} \tag{3.3}$$

With this formulation, however, we are hindered by the fact that the luminance axis is not in the geometrical centre of the space. The grey colours are therefore not at an equal distance from the

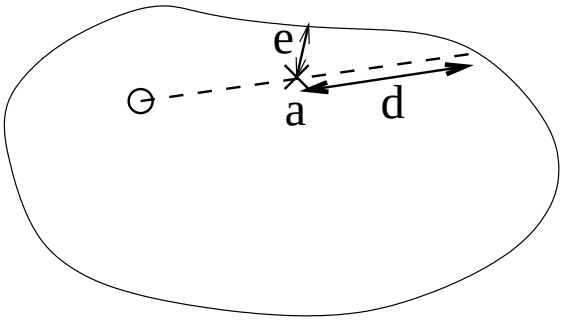

Figure 3.1.: An illustration of the principal disadvantage of the first distance method proposed.

extremal points for all the colours. Thus the colours assigned the highest weights do not coincide with the luminance axis. This leads to the undesired effect of sometimes assigning a non-grey colour a higher weighting than a grey on the luminance axis.

The third approach tried is to make use of two-dimensional homothetic functions in the planes perpendicular to the luminance axis. A homothetic function is defined so that, if we denote by d_j the distance from the centre to the extremal point at angle j, the x-homothetic function passes through all the points xd_j, where $0 \leq j \leq 360$ and $0 \leq x \leq 1$. The weight of a colour is simply taken to be $(1 - x)$. With this approach, we cannot take the extremal points correctly into account — Every point on the envelope surrounding the colour gamut is given a minimum weight of zero.

3.2.2. Electrical potential

The best solution found is to take the weighting as the value of a $\frac{1}{r}$ potential in the L*a*b* space. We choose to model this as an electrostatic potential obtained by placing "charges" at various astutely chosen positions. Note that the electrostatic potential model is chosen for convenience. We are in no way modelling a physical situation, only making use of a concept which is well understood to simplify the problem at hand. We therefore do not make use of any units or constants from electrostatic theory. One could just as easily visualise this model in terms of gravitational potential, but with negative masses allowed. The actual numerical values of the potential are not important, only the order which they impose on the colours.

The potential is set up in the L*a*b* space by placing a line of positive "charge" on the luminance axis, thereby ensuring that the surrounding greys have the highest potential; and placing negative "charges" at the extremal points, imposing minima on the potential field. This configuration is illustrated in figure 3.2.

General expressions for the potential

The potential due to a line charge can be determined analytically, as is shown in appendix B. Given a positively-charged line of length l, and a point on the line at a distance x from the line

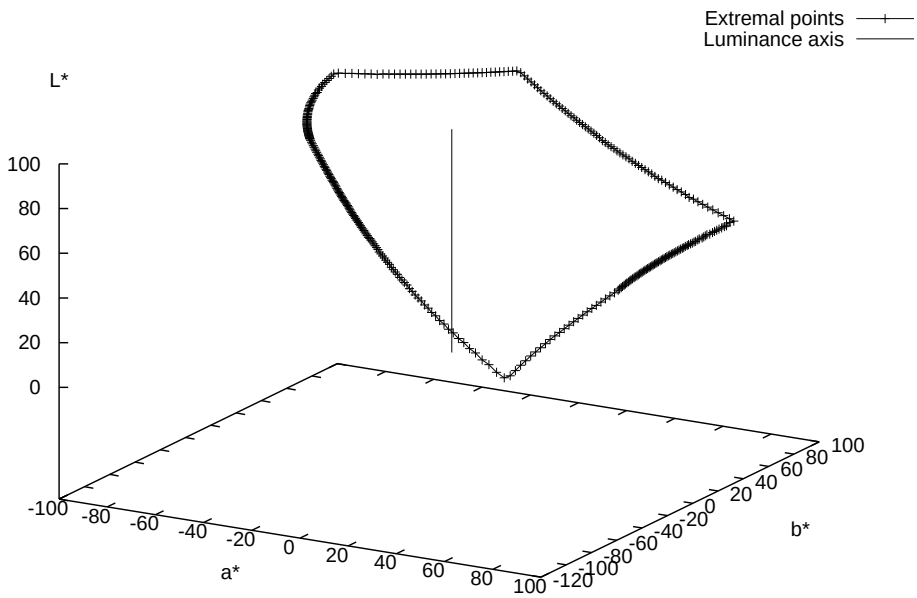

Figure 3.2.: The distribution of “charges” in the L*a*b* space. The line at the centre represents the positive charges on the luminance axis, and the surrounding ring is the negative charges at the extremal points.

centre, the potential V_+ at a point with a perpendicular distance of d from point x on the line charge is

$$V_+ = \lambda \ln \left[b + \sqrt{b^2 + d^2} \right] - \lambda \ln \left[-a + \sqrt{a^2 + d^2} \right] \tag{3.4}$$

where λ is the charge per unit distance, $a = \frac{l}{2} - x$ and $b = \frac{l}{2} + x$. Note that for a numerical implementation, it is not advisable to combine the two log terms into one, as this leads to numerical instability.

For the potential due to the negative charges at the extremal points, we assume that a charge $-q_j$ is placed at every integer hue degree $j = 0, 1, \ldots, 358, 359$, so that the total potential V_- at an arbitrary point due to these charges is

$$V_- = -\sum_{j=0}^{359} \frac{q_j}{r_j} \tag{3.5}$$

where r_j is the Euclidean distance of extremal point j to the point at which the potential is being calculated.

Adaptation to the L*a*b* space

The values and positions of the charges in the L*a*b* space are, of course, heuristically chosen to produce the most useful potential function for the problem to be solved. As the numerical values of the potentials are not important, the magnitudes of the charges can be adjusted to produce potential values in a useful range.

We first consider the magnitudes of the negative charges q_j. Two "obvious" possibilities exist, either each charge has an equal magnitude, or the magnitude of the charges is proportional to their distance from the luminance axis. In order to compare these two possibilities, a simple calculation in two dimensions is done. In a two-dimensional polar coordinate system (ρ, θ), a positive point charge is placed at the origin, and negative charges are placed at the points $[C_{\text{ext}}(j), j]$, where $j = 0, 1, \ldots 358, 359$. Two sets of equipotential lines are calculated:

1. The charges q_j at the extremal points all have equal magnitude, resulting in the equipotential lines drawn in figure 3.3a.

2. The charges q_j at the extremal points have magnitude proportional to $C_{\text{ext}}(j)$, with equipotential lines drawn in figure 3.3b.

On comparing these two diagrams, it appears as if the second configuration is to be preferred. For this configuration, the equipotential lines near the extremal points are evenly spaced, demonstrating that colours near these extrema will have equal weighting. In addition, the transition from the equipotential lines following the shape of the extrema to the circular ones near the centre is smoother.

With the luminance axis, we aim to give a slight preference to lighter greys. This is accomplished by using a positively charged line of length 200 luminance units, with the $L^* = 0$ point of the luminance axis placed at the centre of this line. The effect of this line charge is best

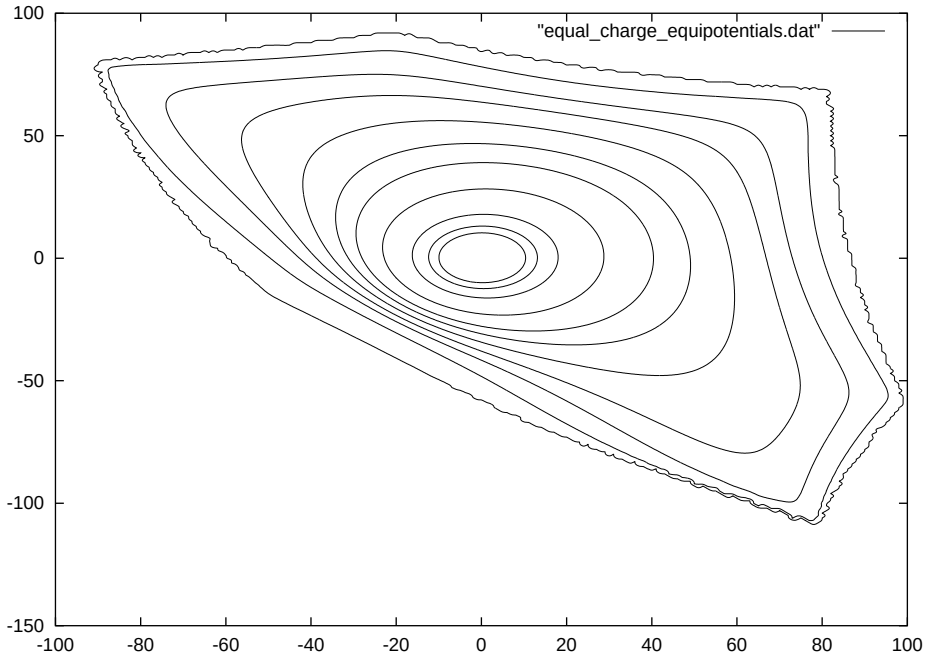

(a)

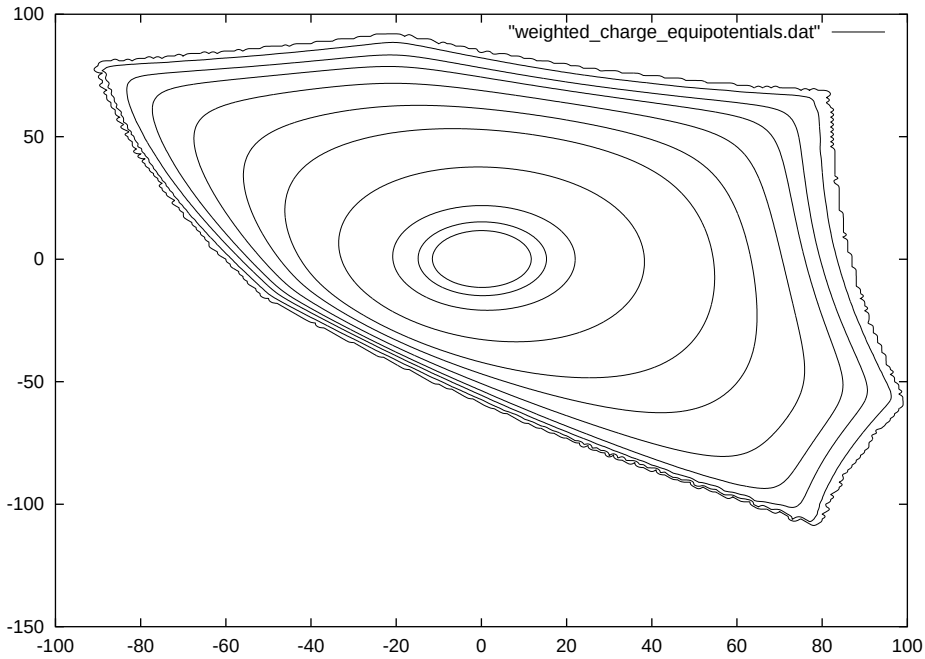

(b)

Figure 3.3.: The equipotential lines with (a) equal charges at the extremal points, and (b) charges proportional to the distance from the origin at the extremal points.

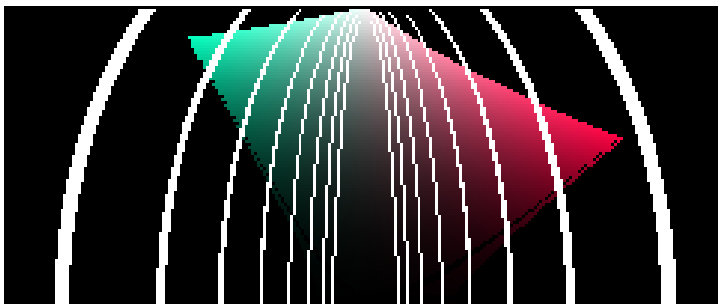

Figure 3.4.: The equipotential lines due only to a line charge placed on the luminance axis.

appreciated by looking at vertical slices parallel to and passing through the luminance axis of the L*a*b* space. Such a slice showing hues with value $0°$ on the right, and $180°$ on the left is shown in figure 3.4. Equipotential lines have been superimposed on the space (the values of the potential falling on a line are equal). They are due only to the positively charged line on the luminance axis, so the potential decreases as one moves further from the centre.

Charge configuration chosen

For the L*a*b* space, the positive charge on the luminance axis and the negative charges at the extremal points are combined to create a potential function in the space as described here. At the point i with coordinates $(L^*, h^*, C^*)_i$, the potential due to the positive line charge is calculated using equation 3.4 with $\lambda = 1$, $l = 200$, $x = L_i^*$ and $d = C_i^*$. The potential due to the negative charges at the extremal points is calculated using equation 3.5, with $q_j = \frac{C_{\text{ext}}(j)}{100}$ and r_j given by equation 2.2 as

$$r_j = \left\{[L_{\text{ext}}(j) - L_i^*]^2 + C_i^* + C_{\text{ext}}(j) - 2 \times C_i^* \times C_{\text{ext}}(j) \times \cos[h_i^* - j]\right\}^{\frac{1}{2}}$$

The weighting at point i is then taken as the sum of these two potentials, or

$$w_i = V_+ + V_- \tag{3.6}$$

Some diagrams of the equipotential lines in the L*a*b* space due to this charge distribution are shown in figure 3.5. Each image shows a slice along a vertical plane of the L*a*b* space parallel to and passing through the luminance axis, and hence showing colours corresponding to two hue values: θ to the right of the axis, and $\theta + 180°$ to the left.

3.3. Basic operations

The use of the weighting function in morphological operations is demonstrated. The supremum of a set of points corresponds to the most highly saturated colour, and hence to the point with the lowest weight. Conversely, the infimum is the point with the maximum weight. The two images used in the examples in this section, the LIZARD and MIRO images, are shown in figures 3.6a and b.

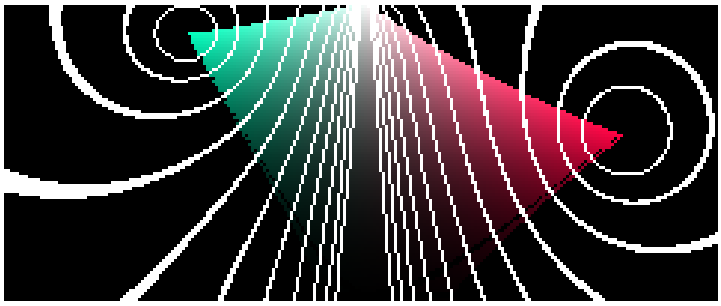

(a) 180° – 0°

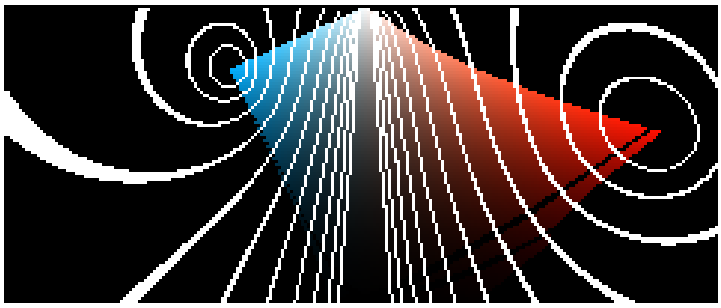

(b) 225° – 45°

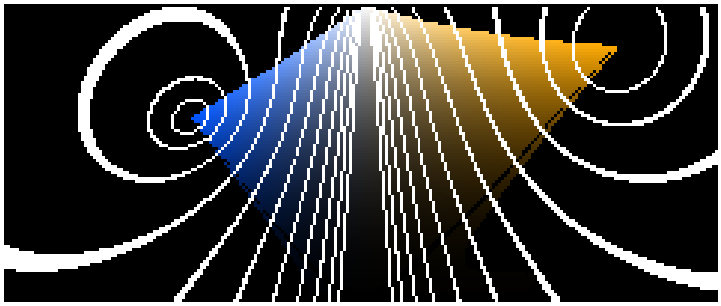

(c) 270° – 90°

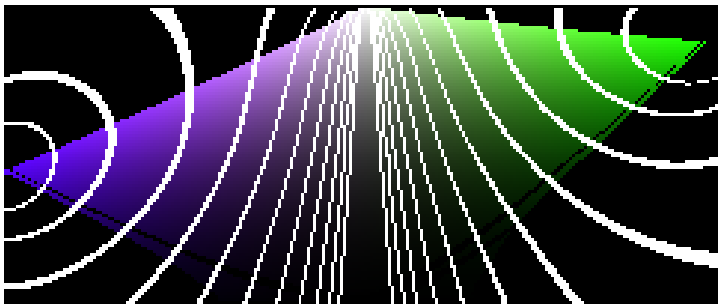

(d) 315° – 135°

Figure 3.5.: The equipotential lines for some vertical slices through the L*a*b* space. The hue values on the left and right of the luminance axis are given below each image.

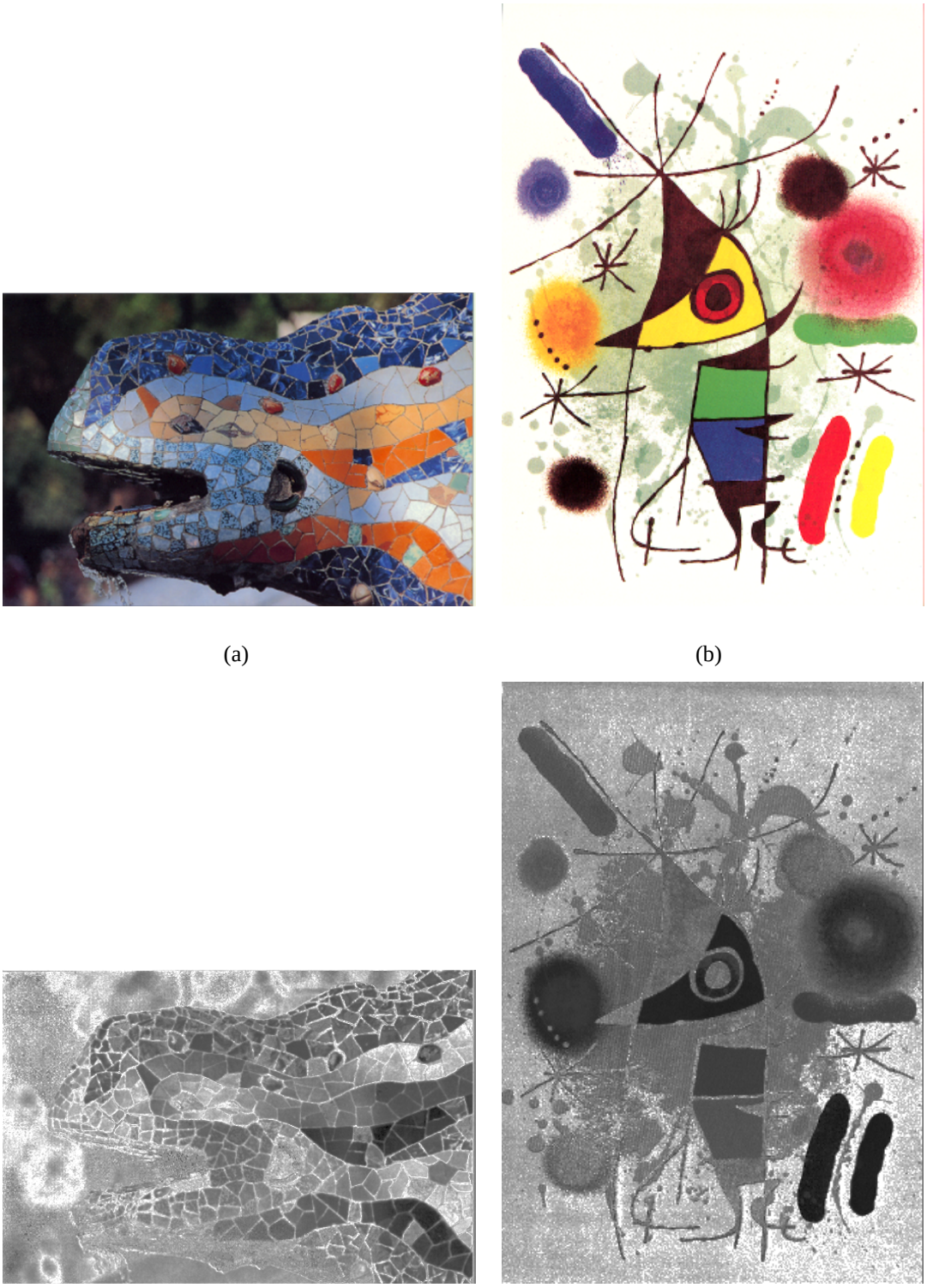

Figure 3.6.: The example images (a) LIZARD — a lizard statue in Barcelona (size 544×360 pixels) and (b) MIRO — "Le Chanteur" by Joan Mirò (size 296×418 pixels). (c) and (d): The potential functions for images (a) and (b).

3.3.1. Colour order

The weight (equation 3.6) is calculated for each colour vector in the L*a*b* space. A weight image corresponding to a colour image is produced by replacing each colour pixel with its corresponding weight. The two weight images corresponding to figures 3.6a and b are shown in figures 3.6c and d, where the grey-level represents the weight of the colour vector, and hence darker pixels indicate colours which are closer to the extremal points.

With the potential function approach, we have created a lattice of equipotential *surfaces*. The colour vectors making up an equipotential surface have not yet been ordered. Unfortunately, the best order for the colour vectors in the same equipotential surface is not obvious. In order to obtain a complete ordering of the colour vectors, we make use of the lexicographical order. The order of the equipotential surfaces is placed in the first level, followed by an arbitrary ordering of the vectors in the same equipotential surface in the second and lower levels.

The following lexicographical orders for vectors $\mathbf{c}_i$ and $\mathbf{c}_j$ are introduced

$$\mathbf{c}_i > \mathbf{c}_j \text{ if } \begin{cases} w_i < w_j \\ \text{or} \\ w_i = w_j \quad \text{and} \quad L_i > L_j \\ \text{or} \\ w_i = w_j \quad \text{and} \quad L_i = L_j \quad \text{and} \quad (h_i^* \div h_0^*) < \left(h_j^* \div h_0^*\right) \end{cases} \tag{3.7}$$

and

$$\mathbf{c}_i < \mathbf{c}_j \text{ if } \begin{cases} w_i > w_j \\ \text{or} \\ w_i = w_j \quad \text{and} \quad L_i < L_j \\ \text{or} \\ w_i = w_j \quad \text{and} \quad L_i = L_j \quad \text{and} \quad (h_i^* \div h_0^*) > \left(h_j^* \div h_0^*\right) \end{cases} \tag{3.8}$$

where h_0^* is the hue origin chosen by the user, and

$$a_1 \div a_2 = \begin{cases} |a_1 - a_2| & \text{if} \quad |a_1 - a_2| \leq 180^\circ \\ 360^\circ - |a_1 - a_2| & \text{if} \quad |a_1 - a_2| \geq 180^\circ \end{cases} \tag{3.9}$$

These two extra levels in the order relation are sufficient to completely order the colour vectors as long as there are no *spherical* equipotential surfaces contained in the colour gamut. If use is made of a charge configuration resulting in a spherically shaped equipotential surface included in the colour gamut, then a fourth level relation for C^* would be necessary to retain the complete ordering.

In a practical application of a morphological operator, the value of h_0^* is not critical, as it is very seldom used, a phenomenon discussed further in section 3.5.

Note that the use of equation 3.9 does not directly result in a complete order, as is explained in the following example. Two points $a_1 = a_0 + (\theta \div a_0)$ and $a_2 = a_0 - (\theta \div a_0)$, where θ is an arbitrary angle, have the same distances from the origin, even though they are not the same point. We can impose a complete order by stating, for example, that in the situation where $a_1 \div a_0 = a_2 \div a_0$ and $a_1 \neq a_2$, we take $a_1 > a_2$ if $(a_1 \mod 360^\circ) < 180^\circ$, else $a_1 < a_2$.

3.3.2. Operators

Once these orders have been defined, the morphological operators are defined in the standard way. The vector erosion at point $\mathbf{x}$ by structuring element B is

$$\varepsilon_B f(\mathbf{x}) = \{f(\mathbf{y}) : f(\mathbf{y}) = \inf[f(\mathbf{z})], \mathbf{z} \in B_{\mathbf{x}}\} \tag{3.10}$$

and the corresponding dilation by structuring element B is

$$\delta_B f(\mathbf{x}) = \{f(\mathbf{y}) : f(\mathbf{y}) = \sup[f(\mathbf{z})], \mathbf{z} \in B_{\mathbf{x}}\} \tag{3.11}$$

An opening γ_B is an erosion followed by a dilation, and a closing φ_B is a dilation followed by an erosion.

3.3.3. Examples

The first example demonstrates the behaviour of these operators. The LIZARD image was purposely chosen as it contains highly coloured regions — the mosaic tiles — separated by grey lines. The result of the erosion, dilation, opening and closing operators are shown in figure 3.7. The operators produce the expected results, with the dilation operator enlarging the tiles, and the erosion operator enlarging the regions between the tiles.

The second set of examples in figures 3.8 and 3.9 serve to illustrate the similarities and differences between the approach presented for images in the L*a*b* space, and the analogous approach in the HLS space of the lexicographical order with saturation in the first position [7]. The MIRO image used in the example is more demanding than the LIZARD image as it contains black and white regions in addition to the coloured regions.

The results of the two approaches are strikingly similar, with the colours always being chosen in preference to the black, white and grey pixels for the dilation operator. The main differences are found when pixels of similar grey level or colours of similar saturation are ordered. The effects of the operators near the image borders have not been standardised, so the results in these regions should be ignored.

3.4. Top-hat

One can create an operator analogous to the greyscale top-hat [12] for use on image in the L*a*b* space. The greyscale opening top-hat is defined as

$$\mathrm{TH}^{\mathrm{g}}_{\gamma}(\mathbf{x}) = f(\mathbf{x}) - \gamma^{\mathrm{g}}_{B}(\mathbf{x})$$

for all points $\mathbf{x}$ in f, and the greyscale closing top-hat is defined as

$$\mathrm{TH}^{\mathrm{g}}_{\varphi}(\mathbf{x}) = \varphi^{\mathrm{g}}_{B}(\mathbf{x}) - f(\mathbf{x})$$

.

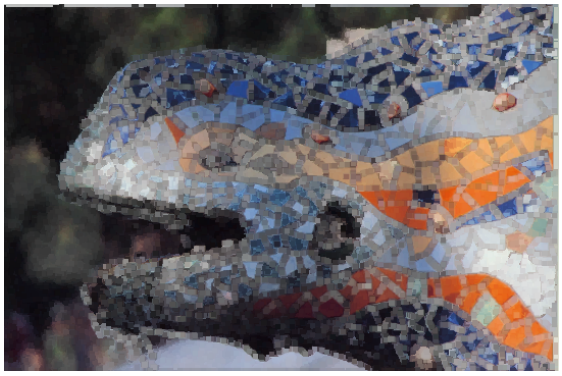

(a) erosion

(b) dilation

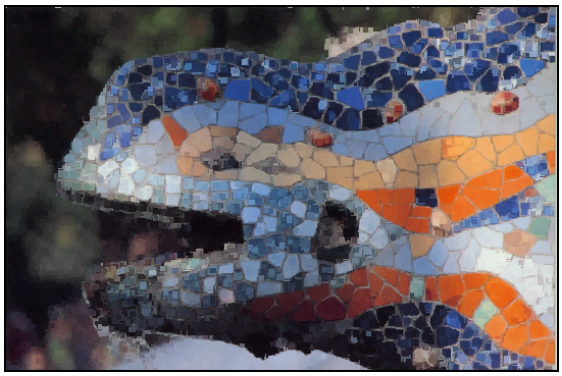

(c) opening

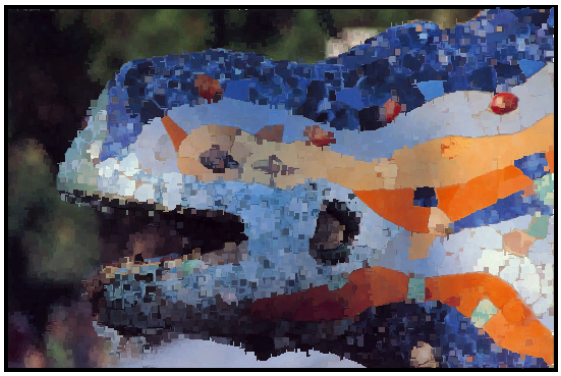

(d) closing

Figure 3.7.: An (a) erosion, (b) dilation, (c) opening and (d) closing of the LIZARD image with a square structuring element of size 2 (5×5).

(a) L*a*b* erosion

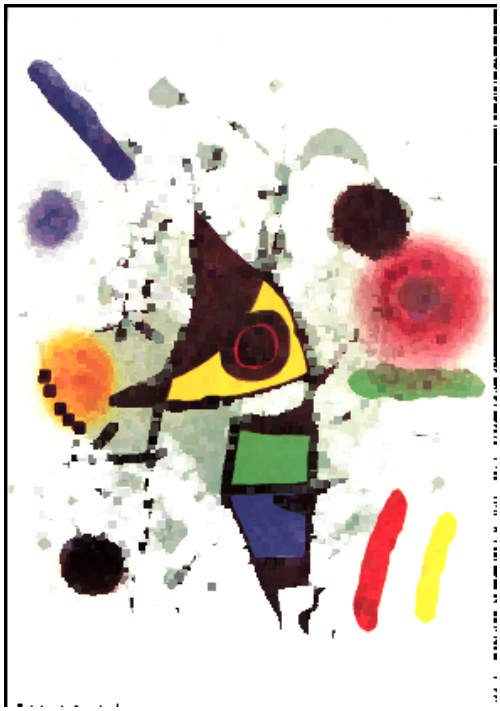

(b) HLS erosion

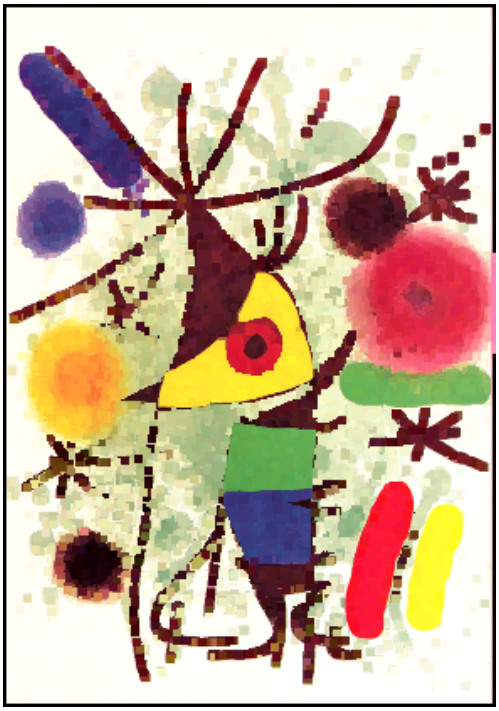

(c) L*a*b* dilation

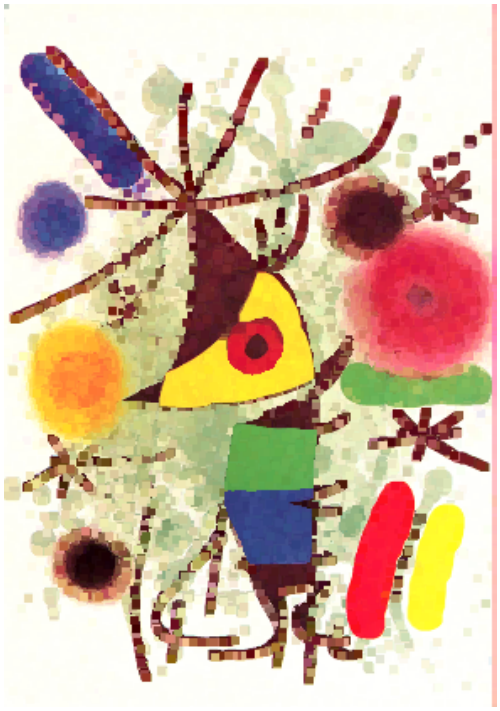

(d) HLS dilation

Figure 3.8.: The MIRO image eroded in the (a) L*a*b* and (b) HLS spaces, and dilated in the (c) L*a*b* and (d) HLS spaces with a structuring element of size 2.

(a) L*a*b* opening

(b) HLS opening

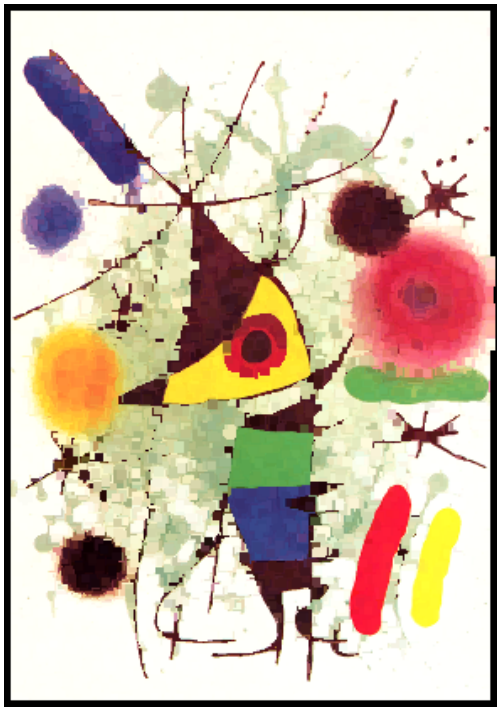

(c) L*a*b* closing

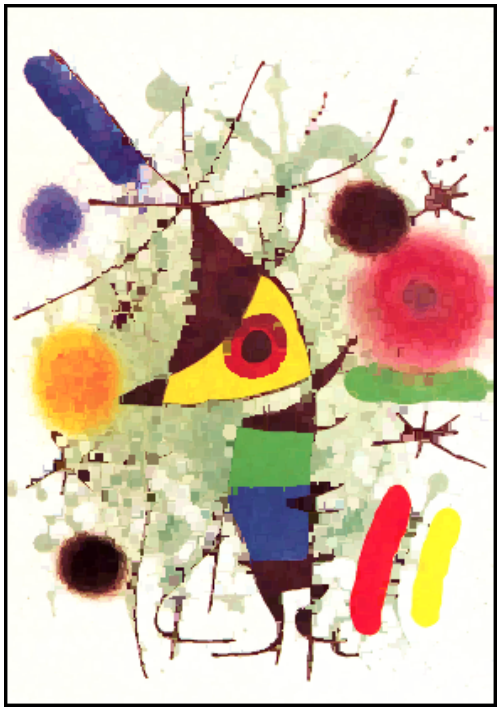

(d) HLS closing

Figure 3.9.: The MIRO image opened in the (a) L*a*b* and (b) HLS spaces, and closed in the (c) L*a*b* and (d) HLS spaces with a structuring element of size 2.

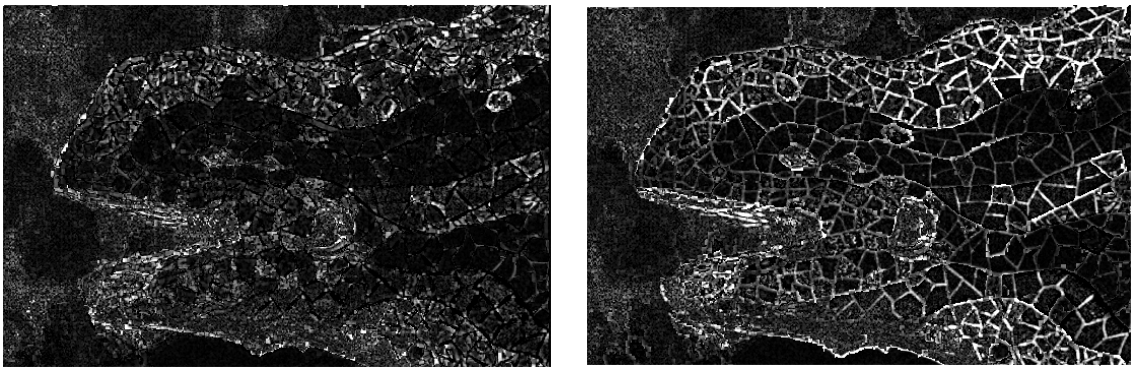

(a) opening top-hat (b) closing top-hat

Figure 3.10.: The (a) opening and (b) closing top-hats of the LIZARD image with a square of size 2.

The L*a*b* space top-hat introduced here produces a greyscale image which encodes the colour distances between pixels in the initial L*a*b* colour image and either its opening or closing. The opening top-hat is

$$\mathrm{TH}_{\gamma}(\mathbf{x}) = \Delta E^{*}_{ab}\left\{f(\mathbf{x}), \gamma_{B} f(\mathbf{x})\right\}$$

and the closing top-hat is

$$\mathrm{TH}_{\varphi}(\mathbf{x}) = \Delta E^{*}_{ab}\left\{f(\mathbf{x}), \varphi_{B} f(\mathbf{x})\right\}$$

for all points $\mathbf{x}$ in f, where the notation $\Delta E^{*}_{ab}\left\{\mathbf{c}_i, \mathbf{c}_j\right\}$ indicates the colour (Euclidean) difference between vectors $\mathbf{c}_i$ and $\mathbf{c}_j$ (equations 2.1 and 2.2). Notice that as the distance is always positive, the order of the images in the subtraction does not matter.

An example of an opening and closing top-hat on the LIZARD image is shown in figure 3.10. The closing top-hat, as expected, extracts the lines between the mosaic tiles. The intensity of the pixels is proportional to the colour distance between the tiles and the lines surrounding them.

3.5. Lexicographical order statistics

When applying a morphological operator based on the lexicographical order described by relations 3.7 and 3.8, it is useful to know the proportion of comparisons for which a decision on vector order is made based only on the first level, and the number of times the relations in the second and third levels need to be used. This is especially important given that in the third level, there is a parameter h^{*}_{0} set by the user, and the effect of this parameter on the final result depends on the number of times the third level of the relation is used.

An experiment counting the number of times each level of the relation was used in a comparison between colour vectors was thus performed. A morphological operation on an image of

size $m \times n$ pixels with a square structuring element of size s requires $m \times n \times (2s+1)^2$ vector comparisons. For an image, the number of times each level was invoked to resolve a comparison was counted, as well as the number of times a comparison was done on two identical vectors. As we are dealing with floating-point images, it is necessary to define the largest difference between two floating-point numbers which are considered to be equal, that is, for two arbitrary numbers a and b, $a = b$ if $|a - b| < \delta$. For the results below, we used $\delta = 10^{-6}$.

The experiments were performed on five images, and the erosion, dilation, opening and closing operators with a square of size 2 were applied to each image. The images are MIRO and LIZARD used above; and CUGAT, FRUIT and FIFER which are shown in appendix C.

The results are shown in table 3.1. The image name and number of comparisons are given in the first column. The second column lists the four operators applied to each image. The third operator is a dilation of the eroded image to produce an opened image, and the fourth operator is an erosion of the dilated image to produce a closed image. The third column shows the percentage of comparisons which were resolvable using only the first level of the lexicographical relation, and the fourth column shows the percentage of comparisons for which, after passing through the three levels, the vectors turned out to be identical. The fifth and sixth columns show the *number* of times that use was made of the second and third level relations to resolve the order of two non-identical vectors.

For the images in the experiment, the third level relation is never used, so the value of h_0^* has no effect on the results. The second level relation is used only a negligible number of times. As one would predict, the number of comparisons of identical pixels is larger when an operator is applied to an image which has already been eroded or dilated (i.e. for the second step in the opening or closing operators).

Even though it appears that the second and third levels can be removed without loss, it would be simple to modify the order relation so that they play a more important part. If we coarsen the weighting function by limiting its output to a finite number n of integer values (i.e. by using a step function), then the utilisation of the second and third levels in the decision process is related to the value of n. If n is small, then the second and third level relations will be needed more often to resolve the order of a larger number of vectors having equal weights.

3.6. Rotational invariance

By rotational invariance, we mean that the results are invariant to a change of position of the hue origin. If we, for example, move the hue origin from the red segment of the hue circle to the blue segment, we would ideally like the colour order to remain the same.

In the HLS space, the lexicographical order with saturation at the first level [7] is described by the relation

Image and number of comparisons	Operator	Percentage 1st level	Percentage identical	Number 2nd level	Number 3rd level
MIRO	Erosion	91.1	8.9	1	0
3061850	Dilation	96.3	3.7	4	0
	Dilation of erosion	57.1	42.9	10	0
	Erosion of dilation	71.9	28.1	0	0
LIZARD	Erosion	99.6	0.4	13	0
4896000	Dilation	99.3	0.7	4	0
	Dilation of erosion	80.5	19.5	3	0
	Erosion of dilation	79.6	20.4	0	0
CUGAT	Erosion	97.0	3.0	2	0
2939200	Dilation	95.7	4.3	1	0
	Dilation of erosion	77.6	22.4	8	0
	Erosion of dilation	74.7	25.3	0	0
FRUIT	Erosion	99.5	0.5	2	0
773850	Dilation	98.9	1.1	1	0
	Dilation of erosion	80.9	19.1	0	0
	Erosion of dilation	79.0	21.0	5	0
FIFER	Erosion	83.0	17.0	0	0
2662500	Dilation	89.9	10.1	0	0
	Dilation of erosion	46.4	53.6	0	0
	Erosion of dilation	55.2	44.8	0	0

Table 3.1.: The results of the experiment counting the number of times each level of the order relation is used for five images.

$$\mathbf{c}_i > \mathbf{c}_j \quad \text{if} \quad \begin{cases} S_i > S_j \\ \text{or} \\ S_i = S_j \quad \text{and} \quad |L_i - 0.5| < |L_j - 0.5| \\ \text{or} \\ S_i = S_j \quad \text{and} \quad |L_i - 0.5| = |L_j - 0.5| \quad \text{and} \quad H_i \div H_0 < H_j \div H_0 \end{cases} \tag{3.12}$$

The first two levels of this relation are obviously independent of the choice of the hue origin H_0. The hue only enters into the third level relation, and given the results of section 3.5, one may be tempted to ignore this parameter as in practice it has little or no effect on the outcome of the morphological operators. On the other hand, if we consider the complete ordering of all the vectors in the HLS space, it is clear that the resulting order depends critically on the value of H_0.

The lexicographical order suggested for the L*a*b* space is similar to the above HLS space order, and also consists of two levels which are rotationally invariant, and a third level depending on the hue. These levels can be summarised as:

1. Order of equipotential surfaces (rotationally invariant).

2. Order of the luminance within each equipotential surface (rotationally invariant). This level is in fact the order of a set of one-dimensional rings tracing out lines of equal potential and equal luminance.

3. Order by hue within each equipotential equi-luminance ring (depends on the choice of a hue origin).

In conclusion, the approach adopted in this report is to make the morphological operators as "rotationally invariant as possible". We do this by placing the relations which depend on the choice of an origin in positions which have been experimentally shown to be almost never used, so that in practice, their effect is almost negligible.

An alternative approach would be to start with operators which are designed to be rotationally invariant on the hue, such as those introduced in [8], and add ways for them to take the other vector components into account. This remains to be explored.

4. Conclusion

The use of a weighting function to impose an order on colours in the L*a*b* space is presented. After introducing the theory underlying the use of a weighting function in the context of a vector space, the electrostatic potential model is used as a basis for creating a weighting function which simulates an order by colour saturation in the L*a*b* space. The weighting function has the advantages of taking the positions of the luminance axis and extremal colours into account, and being adaptable to many L*a*b* colour gamuts. The development of such a weighting function is useful in that it avoids the necessity to transform to another colour space, an action possibly accompanied by loss of colour information, before applying morphological operators based on an order by saturation. This is well demonstrated by the top-hat example, where we initially ignore the inherent characteristics of the L*a*b* space by imposing an order based on colour saturation, and then make intensive use of the perceptual uniformity characteristics during the subtraction step.

The adaptation of the weighting function to other colour gamuts can be done by following the steps presented in this report. One begins with the transformation of an RGB colour cube completely filled with points to the L*a*b* space, after which the position of the extremal points of the resultant colour gamut are found. The negative charges are placed at these extremal points, and, not forgetting to take the positive charge on the luminance axis into account, the weight of each colour can be determined.

The way in which the charge distribution at the extremal points is modelled should be improved. At the moment, the irregularly-shaped curve on which the extremal points are found is approximated by a line of point charges. A formulation allowing these charges to be represented as a continuous line charge, as for the line at the centre, will improve the results for highly saturated colours. The calculation time of the weighting function is not critical, as the weight of each colour only has to be calculated once for each colour gamut, after which a three-dimensional look-up table can be used. An accurate implementation of the weighting function calculation should therefore be possible.

This improvement in the accuracy of the weight calculation is necessary before this formulation can be used for morphological reconstruction operators. With the current approximation of the negatively charged line by relatively widely spaced point charges, some fully saturated colours have lower weights than others, and one can therefore have an “invasion” of an image by certain colours during a reconstruction process.

A possible useful modification to this technique could be to change the potential function by adding charges elsewhere in the space. For example, if one is interested in regions of a specific colour, an additional negative point charge could be placed at the position of this colour

in order to modify the shape of the potential function. One would then still have the framework potential function so that colours not affected by the new charge would continue to be treated in a predictable way.

When designing colour morphological operators, one would ideally like them to be completely rotationally invariant so that they do not depend at all on the choice of a hue origin. Here we have adopted the approach of sweeping the problem of rotational invariance as far under the carpet as it will go, by placing the dependence on the hue origin in the third level of a lexicographical order relation. Thus, the position of this origin is critical when ordering all the vectors in the space, but as can be demonstrated experimentally, almost never taken into account when applying morphological operators to images.

A. Colour space conversions

The transformation from the RGB to the L*a*b* space requires a passage through the XYZ space. It is during the transformation from RGB to XYZ that the characteristics of the image capture or display device and the illumination conditions are taken into account. A derivation of the transformation from the RGB to XYZ colour space is given in section A.1, and shows how any set of primaries and white point can be taken into account. For people pressed for time, a matrix for transforming from RGB to XYZ for a set of commonly used primaries and white point is given in section A.2. The other necessary transformations are XYZ to L*a*b* (section A.3) and the inverse transformations, L*a*b* to XYZ (section A.4) and XYZ to RGB (section A.5). The material in this appendix is mainly from Poynton [11] and Wyszecki and Stiles [16].

A.1. RGB to XYZ derivation

A.1.1. Primaries and white point

We are working in a tristimulus RGB space with primary stimuli

$$\mathbf{R} = \begin{bmatrix} 1 \\ 0 \\ 0 \end{bmatrix}, \quad \mathbf{G} = \begin{bmatrix} 0 \\ 1 \\ 0 \end{bmatrix}, \quad \mathbf{B} = \begin{bmatrix} 0 \\ 0 \\ 1 \end{bmatrix}$$

so that an arbitrary stimulus $\mathbf{Q}$ is written as

$$\mathbf{Q} = R_Q\mathbf{R} + G_Q\mathbf{G} + B_Q\mathbf{B}$$

where R_Q, G_Q and B_Q are called the *tristimulus values*.

In colourimetric practice, a two-dimensional representation is often used, in which the coordinates of the colours in the plane $R + G + B = 1$ are given. These *chromaticity coordinates* are defined as

$$\begin{aligned} r &= \frac{R}{R+G+B} \\ g &= \frac{G}{R+G+B} \\ b &= \frac{B}{R+G+B} \end{aligned}$$

	x	y	z
CIE-R	0.73467	0.26533	0.00000
CIE-G	0.27376	0.71741	0.00883
CIE-B	0.16658	0.00886	0.82456
Rec.709-R	0.640	0.330	0.030
Rec.709-G	0.300	0.600	0.100
Rec.709-B	0.150	0.060	0.790

Table A.1.: The CIE [16] and Rec.709 [11] primary chromaticity coordinates.

	x	y	z
CIE-Illuminant A (tungsten filament lamp)	0.44757	0.40745	0.14498
CIE-Illuminant B (direct sunlight)	0.34842	0.35161	0.29997
CIE-Illuminant C (average daylight)	0.31006	0.31616	0.37378
Rec.709 D_{65}	0.3127	0.3290	0.3582

Table A.2.: The chromaticity coordinates of some CIE standard illuminants [16] and the Rec.709 white point [11].

from which it follows that

$$r + g + b = 1$$

In 1931, in order to overcome certain deficiencies in the RGB system, the CIE introduced a new tristimulus coordinate system, the XYZ system, with corresponding chromaticity coordinates

$$\begin{aligned} x &= \frac{X}{X+Y+Z} \\ y &= \frac{Y}{X+Y+Z} \\ z &= \frac{Z}{X+Y+Z} \end{aligned}$$

were

$$x + y + z = 1$$

The xyz chromaticity coordinates of the three CIE-RGB primary stimuli and the internationally agreed primaries (Rec. 709 [2]) for high definition television (HDTV), which corresponds closely to the primaries used in computer monitors, are given in Table A.1.

In order to completely specify an XYZ coordinate system, the coordinates of the three primary stimuli and the white point must be given. The white point is the colour obtained when the R, G and B tristimulus values are at their maxima. The chromaticity coordinates of some CIE standard illuminants are given in table A.2, along with the coordinates of the Rec. 709 HDTV standard white point. If the white point of an image is not known, there exist methods which can be used to estimate it [3].

The chromaticity coordinates (x_D, y_D) of the CIE D (daylight) illuminants with a correlated colour temperature T_c can be calculated using the following equations [16]: For correlated colour temperatures from approximately 4000K to 7000K:

$$x_D = -4.6070\frac{10^9}{T_c^3} + 2.9678\frac{10^6}{T_c^2} + 0.09911\frac{10^3}{T_c} + 0.244063$$

For correlated colour temperatures from approximately 7000K to 25000K:

$$x_D = -2.0064\frac{10^9}{T_c^3} + 1.9018\frac{10^6}{T_c^2} + 0.24748\frac{10^3}{T_c^2} + 0.237040$$

The y_D coordinate is calculated as

$$y_D = -3.000x_D^2 + 2.870x_D - 0.275$$

The CIE D_{65} daylight illuminant has a correlated colour temperature of approximately 6504K.

A.1.2. Transformation between two systems of primaries

The transformation between any two systems of primaries is linear. The relation between a colour measured in the XYZ system and in the RGB system is

$$\begin{bmatrix} X \\ Y \\ Z \end{bmatrix} = A \begin{bmatrix} R \\ G \\ B \end{bmatrix} \tag{A.1}$$

where A is the 3×3 matrix with columns giving the tristimulus values of the RGB primaries in the XYZ coordinate system

$$A = \begin{bmatrix} X_R & X_G & X_B \\ Y_R & Y_G & Y_B \\ Z_R & Z_G & Z_B \end{bmatrix}$$

The inverse transformation is

$$\begin{bmatrix} R \\ G \\ B \end{bmatrix} = A^{-1} \begin{bmatrix} X \\ Y \\ Z \end{bmatrix}$$

We know the chromaticity coordinates of the primaries. The tristimulus values are written in terms of the chromaticity coordinates as

$$\begin{bmatrix} X_R \\ Y_R \\ Z_R \end{bmatrix} = \rho_R \begin{bmatrix} x_R \\ y_R \\ z_R \end{bmatrix}, \quad \begin{bmatrix} X_G \\ Y_G \\ Z_G \end{bmatrix} = \rho_G \begin{bmatrix} x_G \\ y_G \\ z_G \end{bmatrix}, \quad \begin{bmatrix} X_B \\ Y_B \\ Z_B \end{bmatrix} = \rho_B \begin{bmatrix} x_B \\ y_B \\ z_B \end{bmatrix}$$

so that the matrix A becomes

$$A = \begin{bmatrix} x_R & x_G & x_B \\ y_R & y_G & y_B \\ z_R & z_G & z_B \end{bmatrix} \begin{bmatrix} \rho_R & 0 & 0 \\ 0 & \rho_G & 0 \\ 0 & 0 & \rho_B \end{bmatrix}$$

Hence, from equation A.1

$$\begin{bmatrix} X \\ Y \\ Z \end{bmatrix} = \begin{bmatrix} x_R & x_G & x_B \\ y_R & y_G & y_B \\ z_R & z_G & z_B \end{bmatrix} \begin{bmatrix} \rho_R & 0 & 0 \\ 0 & \rho_G & 0 \\ 0 & 0 & \rho_B \end{bmatrix} \begin{bmatrix} R \\ G \\ B \end{bmatrix} \tag{A.2}$$

At the white point, $R = G = B = 1$, and the luminance is at its maximum value of 1. The tristimulus values of the white point can be written as [16, Table 1(3.3.3)]

$$X_{wp} = \frac{x_{wp}}{y_{wp}}, \quad Y_{wp} = 1, \quad Z_{wp} = \frac{z_{wp}}{y_{wp}}$$

These are inserted into equation A.2 to calculate the values of ρ_R, ρ_G and ρ_B, and hence the 3×3 transformation matrix, i.e.

$$\begin{bmatrix} x_R & x_G & x_B \\ y_R & y_G & y_B \\ z_R & z_G & z_B \end{bmatrix}^{-1} \begin{bmatrix} \frac{x_{wp}}{y_{wp}} \\ 1 \\ \frac{z_{wp}}{y_{wp}} \end{bmatrix} = \begin{bmatrix} \rho_R & 0 & 0 \\ 0 & \rho_G & 0 \\ 0 & 0 & \rho_B \end{bmatrix} \begin{bmatrix} 1 \\ 1 \\ 1 \end{bmatrix}$$

$$\Longrightarrow \begin{bmatrix} \rho_R \\ \rho_G \\ \rho_B \end{bmatrix} = \begin{bmatrix} x_R & x_G & x_B \\ y_R & y_G & y_B \\ z_R & z_G & z_B \end{bmatrix}^{-1} \begin{bmatrix} \frac{x_{wp}}{y_{wp}} \\ 1 \\ \frac{z_{wp}}{y_{wp}} \end{bmatrix}$$

Substituting in the specific values for the Rec. 709 HDTV standard from Tables A.1 and A.2,

$$\begin{bmatrix} \rho_R \\ \rho_G \\ \rho_B \end{bmatrix} = \begin{bmatrix} 0.640 & 0.300 & 0.150 \\ 0.330 & 0.600 & 0.060 \\ 0.030 & 0.100 & 0.790 \end{bmatrix}^{-1} \begin{bmatrix} \frac{0.3127}{0.3290} \\ 1 \\ \frac{0.3582}{0.3290} \end{bmatrix} = \begin{bmatrix} 0.64446 \\ 1.19193 \\ 1.20282 \end{bmatrix}$$

Hence, the transformation matrix

$$\begin{aligned} A &= \begin{bmatrix} 0.640 & 0.300 & 0.150 \\ 0.330 & 0.600 & 0.060 \\ 0.030 & 0.100 & 0.790 \end{bmatrix} \begin{bmatrix} 0.64446 & 0 & 0 \\ 0 & 1.19193 & 0 \\ 0 & 0 & 1.20282 \end{bmatrix} \\ &= \begin{bmatrix} 0.412453 & 0.357580 & 0.180423 \\ 0.212671 & 0.715160 & 0.072169 \\ 0.019334 & 0.119193 & 0.950227 \end{bmatrix} \end{aligned}$$

To demonstrate the effect of the white point on the transformation matrix, the matrix using the Rec. 709 primaries and the CIE-A illuminant is given here

$$A_{\mathrm{CIE-A}} = \begin{bmatrix} 0.760983 & 0.295391 & 0.042093 \\ 0.392383 & 0.590781 & 0.016837 \\ 0.035671 & 0.098464 & 0.221688 \end{bmatrix}$$

A.2. RGB to XYZ

The transformation from RGB into XYZ using the Rec. 709 HDTV primaries and D_{65} white point [11] is

$$\begin{bmatrix} X \\ Y \\ Z \end{bmatrix} = \begin{bmatrix} 0.412453 & 0.357580 & 0.180423 \\ 0.212671 & 0.715160 & 0.072169 \\ 0.019334 & 0.119193 & 0.950227 \end{bmatrix} \begin{bmatrix} R \\ G \\ B \end{bmatrix} \tag{A.3}$$

A.3. XYZ to L*a*b*

The luminance L^* is calculated as

$$L^* = 116 \left(\frac{Y}{Y_{wp}} \right)^{\frac{1}{3}} - 16 \qquad \text{if} \quad \frac{Y}{Y_{wp}} > 0.008856$$

and

$$L^* = 903.3 \frac{Y}{Y_{wp}} \qquad \text{if} \quad \frac{Y}{Y_{wp}} \leq 0.008856$$

The chroma coordinates a^* and b^* are calculated as

$$\begin{aligned} a^* &= 500 \left[f\left(\frac{X}{X_{wp}}\right) - f\left(\frac{Y}{Y_{wp}}\right) \right] \\ b^* &= 200 \left[f\left(\frac{Y}{Y_{wp}}\right) - f\left(\frac{Z}{Z_{wp}}\right) \right] \end{aligned}$$

where

$$f\left(\frac{\alpha}{\alpha_{wp}}\right) = \left(\frac{\alpha}{\alpha_{wp}}\right)^{\frac{1}{3}} \qquad \text{if} \quad \frac{\alpha}{\alpha_{wp}} > 0.008856$$

and

$$f\left(\frac{\alpha}{\alpha_{wp}}\right) = 7.787 \left(\frac{\alpha}{\alpha_{wp}}\right) + \frac{16}{116} \qquad \text{if} \quad \frac{\alpha}{\alpha_{wp}} \leq 0.008856$$

The symbol α represents any of X, Y or Z.

Note that the coordinates of the white point, X_{wp}, Y_{wp} and Z_{wp} are obtained by substituting the point $[R, G, B] = [1, 1, 1]$ into equation A.3. The values obtained are $X_{wp} = 0.950456$, $Y_{wp} = 1.0$ and $Z_{wp} = 1.088754$.

A.4. L*a*b* to XYZ

Note that this conversion from L*a*b* back to XYZ should be used only for visualisation of an image, as information is lost in this conversion. This is because one cannot tell whether the initial values of $\frac{X}{X_{wp}}$ and $\frac{Z}{Z_{wp}}$ were greater than or less than the threshold of 0.008856, and hence which equation was used in the conversion to L*a*b*. In this conversion, we use the fact that when $\frac{Y}{Y_{wp}} = 0.008856$, $L^* = 7.9996$.

If $L^* > 7.9996$ then

$$Y = Y_{wp}\left[\frac{L^* + 16}{116}\right]^3$$

else

$$Y = Y_{wp}\frac{L^*}{903.3}$$

The X and Z coordinates are calculated as

$$X = X_{wp}\left[\left(\frac{Y}{Y_{wp}}\right)^{\frac{1}{3}} + \frac{a^*}{500}\right]^3$$

and

$$Z = Z_{wp}\left[\left(\frac{X}{X_{wp}}\right)^{\frac{1}{3}} - \frac{b^*}{200}\right]^3$$

A.5. XYZ to RGB

The transformation from XYZ to RGB with the same primaries and white point as section A.2 is

$$\begin{bmatrix} R \\ G \\ B \end{bmatrix} = \begin{bmatrix} 3.240479 & -1.537150 & -0.498535 \\ -0.969256 & 1.875992 & 0.041556 \\ 0.055648 & -0.204043 & 1.057311 \end{bmatrix} \begin{bmatrix} X \\ Y \\ Z \end{bmatrix}$$

B. Derivation of the potential due to a line charge

We have a line of linear charge density λ on the x-axis between the points $-a$ and b. The charge per unit length $dq = \lambda dx$. The units are ignored in this derivation.

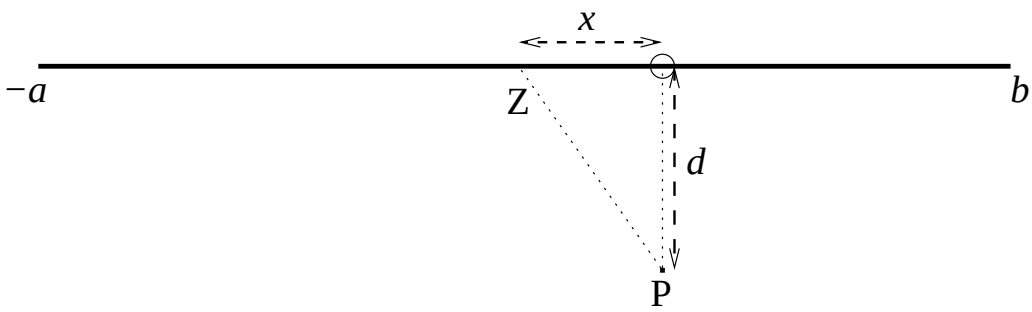

The point P shown is at a distance d perpendicular to the line charge from the origin O. The potential at point P due to the charge on the line at point Z is

$$V_{\mathrm{Z}} = \frac{dq}{\sqrt{x^2 + d^2}}$$

The potential V at point P due to the charge on the whole line is obtained by integrating this expression

$$\begin{aligned} V &= \int_{-a}^{b} \frac{\lambda dx}{\sqrt{x^2 + d^2}} \\ &= \lambda \ln\left(x + \sqrt{x^2 + d^2}\right)\Big|_{-a}^{b} \\ &= \lambda \left[\ln\left(b + \sqrt{b^2 + d^2}\right) - \ln\left(-a + \sqrt{a^2 + d^2}\right)\right] \end{aligned}$$

where the second line is obtained from a table of integrals.

C. Some further results

Some further examples of applications of the lexicographical order described in this report to colour images are presented here. The images are FRUIT, CUGAT and FIFER. On each image, an erosion, dilation, opening and closing has been applied, using a square structuring element of size 2.

(a) original

(b) erosion

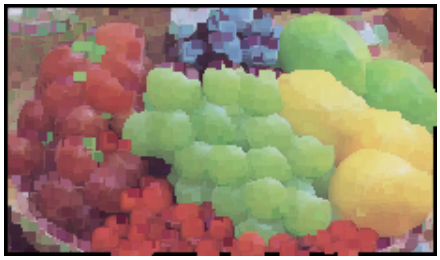

(c) dilation

(d) opening

(e) closing

Figure C.1.: The FRUIT image (size 231×134 pixels).

(a) original

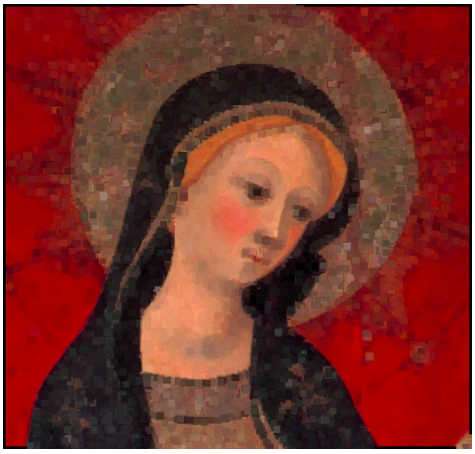

(b) erosion

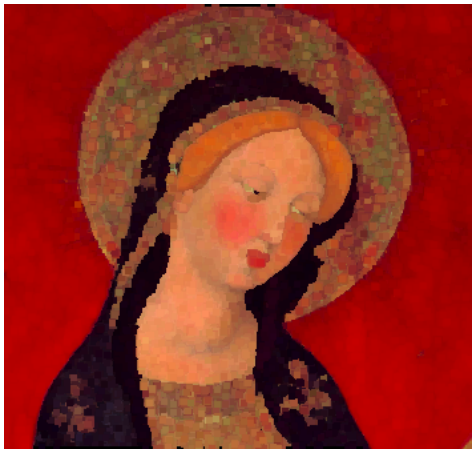

(c) dilation

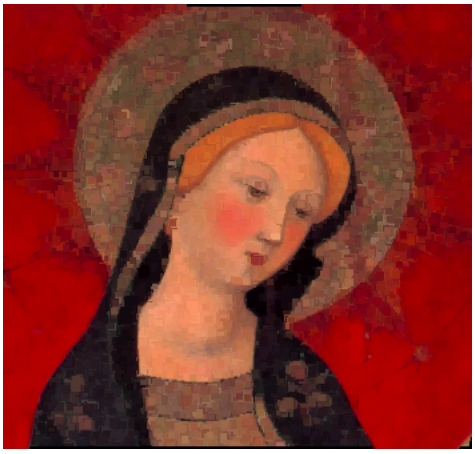

(d) opening

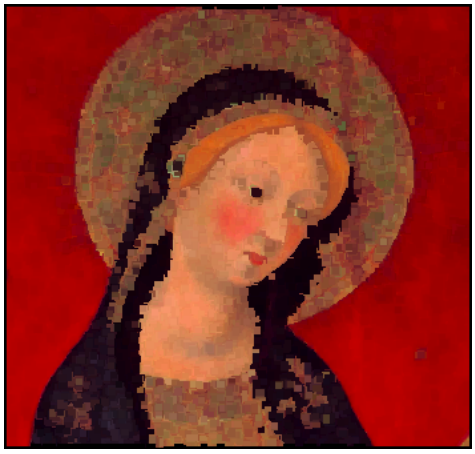

(e) closing

Figure C.2.: The CUGAT image — Virgin by P. Serra, the central panel of a triptych in the Monastery of St. Cugat, Barcelona (size 352×334 pixels).

(a) original

(b) erosion

(c) dilation

(d) opening

(e) closing

Figure C.3.: The FIFER image — “Jouer de Fifre” by E. Manet (size 250×426 pixels).

Bibliography

[1] Heidelberger Druckmaschinen AG. Color manager manual. URL: http://www.linocolor.com/colorman/sp_ciela_2.htm, 2000.

[2] ITU-R Recommendation BT.709. Basic parameter values for the HDTV standard for the studio and for international programme exchange. Geneva: ITU, 1990.

[3] Vlad C. Cardei, Brian Funt, and Kobus Barnard. White point estimation for uncalibrated images. In *Proceedings of the Seventh Color Imaging Conference (CIC'99)*. Imaging Science and Technology Society, November 1999.

[4] J. Chanussot and P. Lambert. Total ordering based on space filling curves for multivalued morphology. In *Proceedings of the International Symposium on Mathematical Morphology (ISMM '98)*, pages 51–58, 1998.

[5] Mary L. Comer and Edward J. Delp. Morphological operations for colour image processing. *Journal of Electronic Imaging*, 8(3):279–289, 1999.

[6] M.C. d'Ornellas, R. Boomgaard, and J. Geusebroek. Morphological algorithms for color images based on a generic-programming approach. In *Proceedings of the XI Brazilian Symposium on Computer Graphics and Image Processing (SIBGRAPI'98)*. IEEE Press, 1998.

[7] Allan Hanbury. Lexicographical order in the HLS colour space. Technical Report N-04/01/MM, Centre de Morphologie Mathématique, Ecole des Mines de Paris, 2001.

[8] Allan Hanbury and Jean Serra. Morphological operators on the unit circle. Accepted for publication by IEEE Transactions on Image Processing.

[9] R. A. Peters II. Mathematical morphology for angle-valued images. In *Non-Linear Image Processing VIII*, volume 3026. SPIE, 1997.

[10] Georges Matheron. Treillis compacts et treillis coprimaires. Technical Report N-5/96G, Centre de Geostatistique, Ecole des Mines de Paris, 1996.

[11] Charles Poynton. Frequently asked questions about color. URL: http://www.inforamp.net/˜poynton/PDFs/ColorFAQ.pdf, 1999.

[12] J. Serra. *Image Analysis and Mathematical Morphology*. Academic Press, London, 1982.

[13] Jean Serra. Anamorphosis and function latices (multivalued morphology). In Edward R. Dougherty, editor, *Mathematical Morphology in Image Processing*, chapter 13, pages 483–523. Marcel Dekker, Inc., 1992.

[14] Pierre Soille. *Morphological Image Analysis: Principles and Applications*. Springer-Verlag, 1999.

[15] H. Talbot, C. Evans, and R. Jones. Complete ordering and multivariate mathematical morphology: Algorithms and applications. In *Proceedings of the International Symposium on Mathematical Morphology (ISMM '98)*, pages 27–34, 1998.

[16] Günter Wyszecki and W.S. Stiles. *Color Science: Concepts and Methods, Quantitative Data and Formulae*. John Wiley and Sons, 2nd edition, 1982.